ChemCatChem

Research Article
doi.org/10.1002/cctc.202300980

Chemistry Europe
European Chemical Societies Publishing

www.chemcatchem.org

Special Collection

Electrocatalytic Functionalized Specialty Paper as Low-Cost Porous Transport Layer Material in CO_2-Electrolysis

Ilias Stamatelos,[a, b] Michael Rentzsch,[c] Chengyu Liu,[d] Franziska Bauer,[c] Stefan Barwe,[e] and Marc Robert*[d, f]

The development of low-cost and efficient electrolyzer components is crucial for practical electrochemical carbon dioxide reduction (ECR). In this study, facile non-woven cellulose-based porous transport layers (PTLs) were developed for high current density CO_2-to-CO conversion. By depositing a cobalt phthalocyanine (CoPc) catalyst-layer over the PTLs, we fabricated ECR-functioning gas-diffusion-electrodes (GDEs) for both flow-cell and zero-gap electrolyzers. Under optimal conditions, the Faradaic efficiency of CO (FE_{CO}) reached 92% at a high current density of 200 mA cm^{-2}. Furthering the architecture of the GDEs, CoPc was incorporated into the initial PTL slurry, forming ECR-active PTLs without the need for an additional catalyst-layer. The new GDE-architecture favored the CoPc-distribution by enhancing the contact and interactions with the carbon substrate and demonstrated a stable electrolysis process for over 50 h in a zero-gap cell at 200 mA cm^{-2} with a FE_{CO} of 80%.

Introduction

The rising content of carbon dioxide in the atmosphere is a growing international concern.[1] The capture and storage of excess atmospheric CO_2 is widely considered a means of decreasing greenhouse gas emissions.[2,3] The electrochemical CO_2 reduction (ECR), coupled with renewable energy sources, is a promising way to utilize supernatural CO_2, converting it into high-value products.[4,5] The products of higher molecular weight (C_{2+}) require multiple proton coupling steps, during the ECR, introducing kinetic inhibitions and higher energy demand.[6–8] Amongst the various ECR products, techno-economic studies indicate that carbon monoxide and formate are the most economically viable products of ECR.[9,10] In addition, CO plays a crucial role as a significant industrial intermediate in the production of numerous chemicals, such as methanol and various synthetic fuels.[11,12]

The high Faradaic efficiency of CO (FE_{CO} >80%) at high current densities (>100 mA cm^{-2}) is important for efficient ECR electrolyzers.[11,13] CO_2-to-CO conversion is preferably catalyzed by noble metals (e.g., Ag, Au), owing to their high stability and FE_{CO}.[14,15] The practical applications of the ECR necessitate the development of efficient catalysts that utilize inexpensive and earth-abundant materials. Various materials, including metal-based oxides, alloys and chalcogenides have been successfully employed for catalyzing the ECR.[16–18] Among them, metal porphyrins and phthalocyanines have emerged as promising catalysts for the CO production.[19,20] This class of materials features high catalytic activity and tenability, relying on earth-abundant metals (e.g., Co, Fe).[21,22] In the early work of Wang et al.,[23] a modified cobalt phthalocyanine (CoPc) recorded an FE_{CO} of 95% in a H-cell. Robert et al.[24] integrated the CoPc catalyst into a gas diffusion electrode (GDE) in a flow-cell electrolyzer, overcoming the previously encountered mass-transfer limitations. They reported a high FE_{CO} of 95% and observed an equally high partial current density for CO (j_{CO}) of 165 mA cm^{-2}. In the same context, Berlinguette et al.[25] noted similar performance in a CoPc catalyst in a zero-gap electrolyzer (in terms of both FE_{CO} and j_{CO}), illustrating the application potential of this material as an efficient ECR catalyst. Despite encouraging performance, CoPc-type catalysts are usually limited by low stability (<20 h), which is due to the harsh reaction conditions in the membrane electrode assembly (MEA) of the electrolyzer.[26]

[a] I. Stamatelos
Institute of Energy and Climate Research
Electrochemical Process Engineering (IEK-14)
Forschungszentrum Jülich GmbH
52425 Jülich (Germany)

[b] I. Stamatelos
Faculty of Mechanical Engineering
RWTH Aachen University
Aachen 52056 (Germany)

[c] M. Rentzsch, F. Bauer
Department of Functional Materials
Business Division Fibers and Composites
Papiertechnische Stiftung
01809 Heidenau (Germany)

[d] Dr. C. Liu, Prof. Dr. M. Robert
Laboratoire d'Electrochimie Moléculaire
Université Paris Cité
CNRS, F-75013 Paris (France)
E-mail: robert@u-paris.fr

[e] Dr. S. Barwe
AIR LIQUIDE Forschung und Entwicklung GmbH
Innovation Campus Frankfurt
60388 Frankfurt (Germany)

[f] Prof. Dr. M. Robert
Institut Universitaire de France (IUF)
F-75005, Paris (France)

Supporting information for this article is available on the WWW under https://doi.org/10.1002/cctc.202300980

Special Collection This publication is part of a Special Collection on "Holistic Development of Electrochemical Processes for Industrial Systems"

The cost of ECR electrolyzers strongly depends on their capital and operational costs (CAPEX and OPEX, respectively), both of which relate to the cost of the catalysts, membrane and porous transport-layers (PTLs) used.[27] Many works revolve around replacing the commonly used iridium-based anode catalyst, which imposes high costs on the electrolyzer's CAPEX.[28,29] The total cost of the MEA is heavily impacted by the cost of the PTL used to form the GDEs of the MEA. The commercially available and commonly used PTLs for the ECR (e.g., Freudenberg, Sigracet) account for 20% of the total CAPEX.[30] The high carbonization temperature (>2000 °C), costly fiber manufacturing process and surface PTFE treatment elevate the cost of PTLs.[31] Modulating their properties is crucial for many electrolysis systems, as their characteristics are known to affect the performance.[32] The early work of Adanur et al.[33] presented the first principles for designing and applying non-woven PTLs to fuel-cells. Kaplan et al.[34] developed PTLs based on cellulose fibers molded under mechanical pressure. Recently, Navarro et al.[35] implemented PTLs made of cotton fibers in an electrolyzer. These works illustrated that the PTL properties can be tuned based on the production technique, benefiting the cost- and energy-efficiency of the MEA. As was shown by Samu et al.[36] the characteristics of the PTLs have a major impact on the performance of an ECR MEA. They demonstrated how features like fiber-orientation, thickness, and the microporous layer influence the CO_2-to-CO conversion. Despite the crucial role of the PTL, no studies have focused on developing facile non-woven PTLs for low-cost ECR applications.

In this study, we developed for the first time paper-PTLs for the CO_2-to-CO conversion, based on cellulose fibers.

Commercial synthetic fibers made of carbon papers and carbon fiber-based nonwovens need to be synthesized by polymerization of acrylonitrile to olyacrylonitrile (PAN), followed by spinning, stabilization and carbonization (typically in the range 1500–2000 °C), film finishing and cutting. In contrast to those cellulose fibers received by the generation of pulp from wood cooking, cleaning and bleaching of bio-polymerized pulp fractions, dewatering, drying and milling is less demanding, which leads to mass-specific price lower by a factor ca. 30. Additionally, precursor impregnation of the carbon papers in compounds like vinyl ester resins with additional tempering treatment for carbonization often at temperatures >2000 °C is necessary, in contrast to the cellulose-based highly filled graphite papers. Furthermore, catalytic functionalization upon direct loading (from a properly formulated suspension) at the beginning of the papermaking process (v30, see next paragraph) offers even more potential for simple process as compared to commercial processing of gas diffusion electrodes by carbon layers comprising catalysts or CCM (catalyst coated membrane) providing. Summarizing the innovation potential of catalytic functionalized highly filled specialty papers can be estimated by both a reduced price and a decrease at least by half of time expenditure.

Our innovative fabrication method not only reduced the production time but also maintained a low-cost advantage for the substrates, making them highly suitable for large-scale applications. To enhance the performance of the PTLs, we carefully tailored their physical-chemical properties by incorporating graphitic carbon micro-structures among the cellulose fibers. This strategic modification imparted the PTLs with desirable hydrophobic characteristics and established a quasi-microporous layer, optimizing their efficiency for CO_2 reduction. Furthering the development of efficient paper-based electrodes, we incorporated the CoPc catalyst directly into the initial PTL slurry. Our strategy resulted in the catalytically active substrate (v30), showcasing remarkable CO_2 reduction capabilities. Notably, v30 demonstrated in the MEA a maximum j_{CO} of 160 mA cm^{-2} and an outstanding ECR stability, continuously operating for 50 hours. Overall, our study presents a significant advancement in the field of CO_2 reduction technology, particularly in the realm of paper-based PTLs. The development of the functionalized v30 material and its successful implementation in ECR electrolyzer configurations highlights a practical and cost-effective approach to CO_2-to-CO conversion. With this innovative research, we pave the way for sustainable and economically viable electrochemical CO_2 reduction processes, advancing green energy technologies.

Results and Discussion

Physical paper characterization

The paper-based PTLs were synthesized by forming a wet-mold slurry, at room temperature, by applying mechanical pressure (Figure S1). The wet-mold includes cellulose fibers, filler, wet-strength agent and internal sizing agent (AKD). The optimization of the PTL's constitution was done gradually, assessing the substrates' different physical and electrochemical properties induced by different component ratios. The cellulose fibers provided the necessary mechanical stability for the substrates. Different ratios of fiber-to-filler content were tested to select the optimal one (Table S1). We identified a fiber content of 20% wt/wt as the optimal one. This fiber-to-filler ratio combines the necessary mechanical strength, air permeability and hydrophobicity (Table S2), which are essential to ensure the PTL's compatibility with the ECR reaction environment in an electrolyzer. The microporous layer plays a vital role in the PTL's ECR performance.[36] In our one-step fabrication process, we created a quasi-microporous layer by adding the filler to the initial slurry. The microporous filler was located within the PTL's fibers (Figure 1a), to create longer and even diffusion pathways for the CO_2. The filler was a mixture of graphitic and spherical carbon microstructures (Figure 1b). For the purpose of optimization, commercial silver nanoparticles were used to compare the effect of the substrate constitution on the ECR performance. Silver is an accessible and already well-established ECR catalyst, therefore used for practical reasons.[9,37] The impact of the different fillers on the ECR performance constitutions was assessed in the flow-cell. We recorded deviations in the cathode's FE_{CO} as a function of the microporous layer's morphology. The ratio of 50/50 graphitic/spherical carbon, exhibited both the highest FE_{CO} (Figure S2a) and the highest partial current density for CO j_{CO} (Figure S2b). Wet-strength

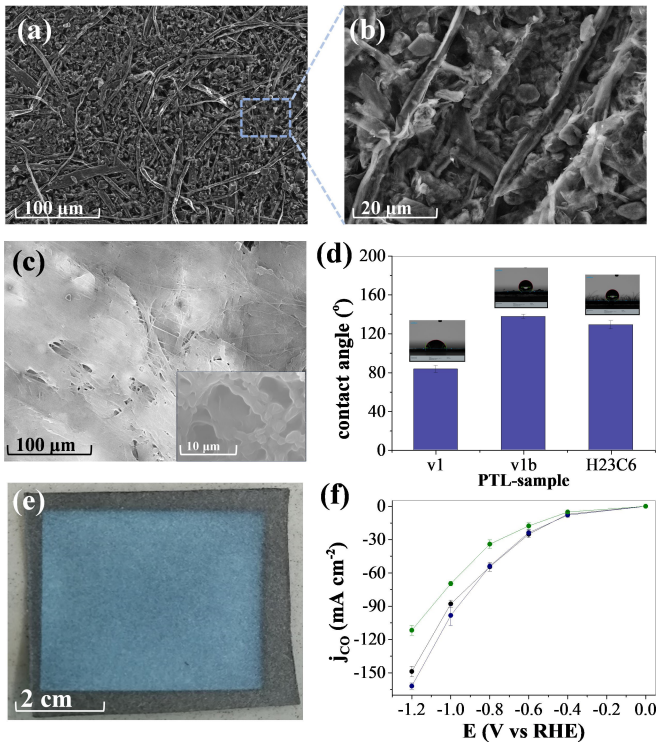

Figure 1. Physical characterization and ECR performance of the optimized PTL samples. (a,b) SEM images of the v1 paper-substrate, (c) SEM image of the v1b substrate, covered with a PTFE layer, (d) Contact angle measurements of the different PTLs, (e) Picture of the PTFE coated v1 sample (v1b), (f) Partial current density for CO (j_{CO}) as a function of the cathode potential for various Ag-coated papers (v1, green; v1b, blue; H22 C6, black) in a flow-cell.

agent and AKD were used to further reinforce the PTL's resilience in aqueous environments. The AKD directly impacts the PTL hydrophobicity, which was assessed in the flow-cell electrolyzer. Absence of AKD resulted in low FE_{CO} and j_{CO} (Figure S2c,d), owing to insufficient hydrophobicity. The AKD concentration of 0.5% wt/wt was seen to exhibit the highest ECR performance with respect to CO formation (Figure S2d). Wet-strength agent of 0.5% wt/wt was thus identified as optimal. This concentration increased the hydrophobicity while maintaining high air permeability (Table S2) necessary for the CO_2 deleverage. The optimization of the content of the PTL's substances led to the formation of our v1 PTL (Figure 1a,b). Recognizing the importance of the surface hydrophobicity for ECR,[38] we sought to further improve the hydrophobic properties of our v1 sample by coating it with PTFE. For our set-up, 30% wt/wt of PTFE was determined to be optimal (Figure S2e,f) and to promote the ECR in the flow-cell. The additional PTFE layer formed a porous overlayer (Figure 1c) covering the initial substrate. The hydrophobicity of the developed sample v1b (Figure 1e) was rapidly increased (Figure 1d). In the flow-cell, the performance of the optimized substrates indicates a high j_{CO} (Figure 1f). The lower j_{CO} of the v1 could be attributed to its lower hydrophobicity in comparison to the v1b and the commercial counterpart (Freudenberg H23 C6). Our F-containing sample (v1b) presented the most promising ECR performance in the electrolyzer, exceeding the performance of the commonly used commercial carbon paper.

Having optimized the structure and composition of the substrates, we sought to further develop the electrode architecture. To employ in our system the PGM-free CoPc, we sought to incorporate the catalyst in the developed v1 substrate. We included the CoPc in the initial slurry forming the ECR-active v30 substrate. The sample maintained a similar surface morphology (Figure 2a) as the initially developed v1 (Figure 1a). The fabrication process of the v30 delivered an even distribution of the CoPc over both the surface of the substrate (Figure 2b) and throughout its cross-section (Figure 2c). The novel architecture of the v30 sample also increased its hydrophobicity (Figure 1d). We attribute the increased hydrophobicity to the presence of the CoPc and its interactions with the PTL (Figure 2e, f). To have a better understanding of the changes induced by the v30 architecture we compared its physical and electrochemical properties with the v1, simply coated with CoPc. The Co-XPS (Figure 2e) suggests that the Co remains in a similar oxidation and electronic state for both the v30 and the CoPc coated v1 GDE (v1/CoPc), suggesting that the properties of the ECR-active Co-center remain similar in both cases. The N-

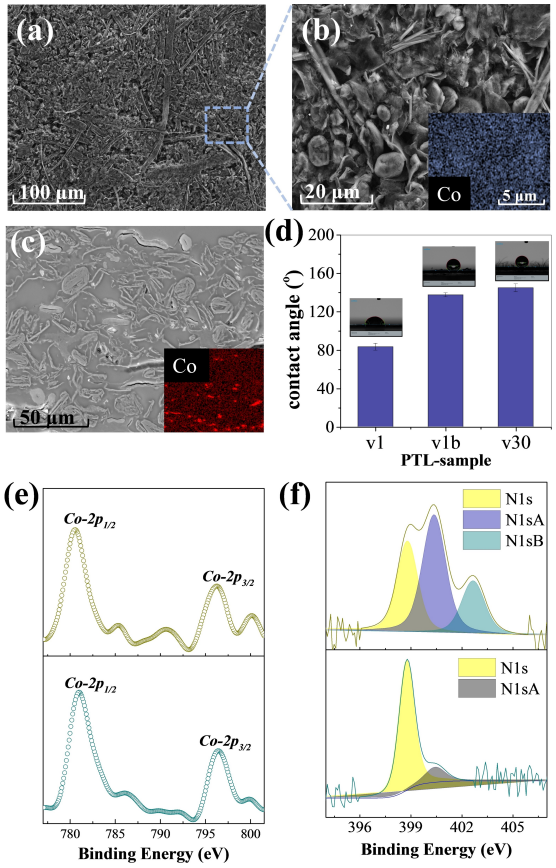

Figure 2. Physical characterizations of the v1 PTL coated with CoPc (v1/CoPc) and the CoPc-functionalized v30 PTL. (a) SEM image of the v30 sample, (b) SEM and EDX of the v30 surface, (c) SEM and EDX of the v30 cross-section, (d) Hydrophobicity (contact angle) of the developed PTLs, (e) High-resolution Co-XPS of the GDEs surface (v30, top panel; v1/CoPc, bottom panel), (f) High-resolution N-XPS of the GDEs surface (v30, top panel; v1/CoPc, bottom panel).

XPS (Figure 2f) initially suggests that both samples exhibit Co–N (N 1s, A) and pyridinic-N (N 1s) interactions, that are related to the structure of the CoPc catalyst.[39] The spectra reveal the additional graphitic-N (N 1s, B) peak, related to the coordination states that only exist in the v30 sample. This state is associated with direct interactions between the N-atoms of the CoPc with the substrate and mostly the filler (graphitic nature).

Electrochemical paper characterization

We initially sought to optimize the CoPc loading for our flow-cell set-up (Figure S3a,b). We determined that a complex loading of 0.65 mg cm^{-2} (6.5 mg cm^{-2} total) delivers the highest ECR activity towards CO. AFM imaging suggested that higher loadings of the catalyst result in a non-homogeneous catalyst layer (Figure S3d), reducing the ECR activity. Lower CoPc loading induces a lower concentration of catalytically active centers. The same CoPc loading (0.65 m^{-2}) was used for all of our PTLs, for comparison reasons and for proof of concept for the advanced v30 architecture. In the flow-cell, the v30 and v1b/CoPc samples exhibited the highest values of FE_{CO} (Figure 3a) owing to the high activity and selectivity of the CoPc and their increased hydrophobicity (Figure 2d).[40] The v1/CoPc GDE presented higher ECR activity than the v30. This behavior is related to the higher CoPc concentration over the v1/CoPc layer (Figure S5a). The v1b/CoPc GDE recorded the highest j_{CO} of −200 mA cm^{-2}, which is associated with its superior hydrophobicity towards the other PTLs (Figure 2d). The high CO selectivity and activity of our substrates in the flow-cell motivated us to test the PTLs' performance in the zero-gap MEA. In the MEA the PTFE-containing v1b exhibited FE_{CO} of 80 % and j_{CO} of 170 mA cm^{-2} at higher overpotential, owing to the interference and resistivity of the additional PTFE layer. The v30 electrode exhibited similar FE_{CO} values while reaching a maximum j_{CO} of 150 mA cm^{-2}. The v30 exhibited lower overpotential owing to its architecture. Indeed, not requiring an additional catalyst layer avoids building up additional charge transfer resistance (R_{ct}) between the PTL and catalyst-layer interface. The lower overall j_{CO} is related to the lower superficial CoPc concentration of the v30 (Figure S5a), since parameters like the air permeability (Table S2) and specific surface area (SSA) (Figure S5d) remain similar for both of the v1 and v30. The v1 GDE featured the highest FE_{CO} of 90 % and maximum j_{CO} of 180 mA cm^{-2}. The activity of the CoPc catalyst and the conductivity of the substrate are responsible for its high ECR activity in the MEA.

Ag-coated vs CoPc-coated vs CoPc-functionalized paper

Up to this point, Ag-nanoparticles were used for the optimization of the substrates, whereas CoPc was used to boost their ECR performance and further the GDE architecture. By comparing the ECR activity of the optimized PTLs, we gain a better understanding of their compatibility with the catalyst materials

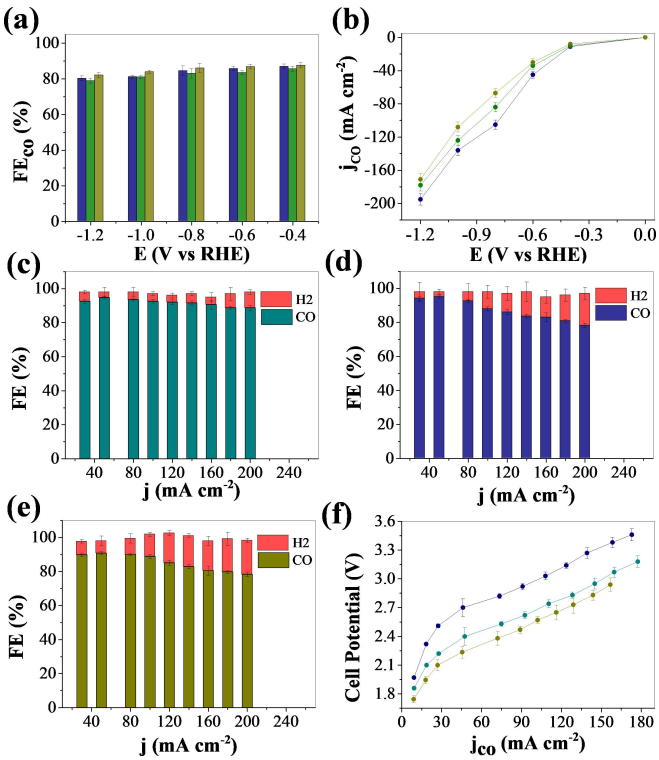

Figure 3. ECR activity of the CoPc-functionalized PTLs. (a) Faradaic Efficiency towards CO (FE_{CO}) of the GDEs (v1/CoPc, light green; v1b/CoPc, blue; v30, greenish brown) in the flow-cell, (b) Partial current densities for CO j_{CO}, of the GDEs (v1/CoPc, light green; v1b/CoPc, blue; v30, greenish brown) in the flow-cell as a function of the cathode potential, (c) Faradaic Efficiency towards CO (FE_{CO}) of the v1 coated with CoPc, in the MEA, (d) Faradaic Efficiency towards CO (FE_{CO}) of the v1b coated with CoPc, in the MEA, (e) Faradaic Efficiency towards CO (FE_{CO}) of the v30 functionalized with CoPc, in the MEA, (f) MEA cell potential as a function of the partial current density for CO (j_{CO}), of the GDEs (v1/CoPc, light green; v1b/CoPc, blue; v30, greenish brown).

of radically different classes. In the flow-cell the v1b/CoPc and the v30 GDEs exhibited the most promising performances, owing mostly to their increased hydrophobicity. The ECR performance (Figure 4a) suggests that the activity depends (v1b) on the catalyst used. Potentiostatic impedance spectroscopy (PEIS) led to similar observations. The decrease of charge transfer resistance (R_{ct}) between the v1b/Ag (21 Ω) and v1b/CoPc (12 Ω) GDEs suggests that the ECR features solely depend on the catalyst's features. The higher HFR (High-Frequency Resistance) of the v1b/Ag (4.8 Ω) is also a result of the higher conductivity of the CoPc catalyst layer. The v30 presents similarly high ECR activity, with its impedance spectra revealing more of its architecture's advantages. The reduced R_{ct} (7 Ω) and HFR (2.1 Ω) are a result of the elimination of the substrate-catalyst layer interface and the additional interactions between the substrate-CoPc complex (Figure 2f). In the MEA the v30 and the v1-based GDEs exhibited the most promising results. The v1/Ag and v1/CoPc exhibited the same maximum j_{CO} (180 mA cm^{-2}) (Figure 4c). Even though CoPc is known to be more CO-selective, the harsh MEA environment is known not to favor the CoPc performance. The higher ECR activity of the CoPc catalyst can though be observed by the lower over-

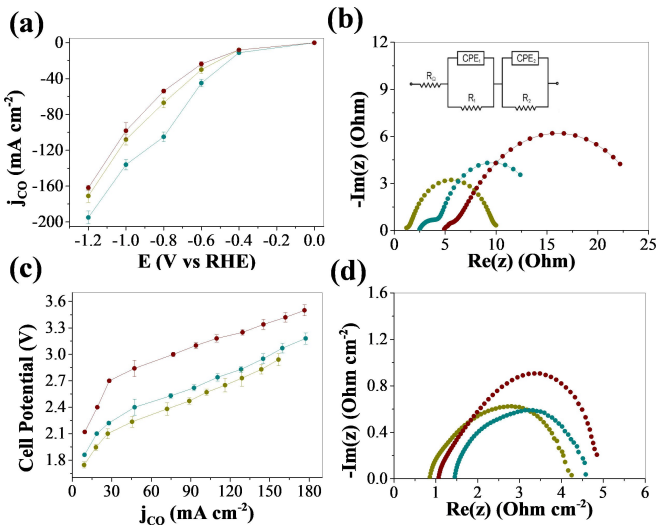

Figure 4. Comparison of the ECR performance and electrochemical characteristics of the optimized PTLs. Characteristics of the CoPc coated v1b (v1b/CoPc), the CoPc-functionalized v30 and the Ag-coated v1b (v1b/Ag). (a) Polarization curves, in terms of j_{CO}, in the flow-cell of the different GDEs (v1b/CoPc, cyan; v30, greenish brown; v1b/Ag, burgundy), (b) Potentiostatic Impedance Spectroscopy (PEIS) of the different GDEs (v1b/CoPc, cyan; v30, greenish brown; v1b/Ag, burgundy), measured on onset potential, in the flow-cell, (c) MEA cell potential as a function of the partial current density for CO (j_{CO}) of the different GDEs (v1b/CoPc, cyan; v30, greenish brown; v1b/Ag, burgundy) (d) Galvanostatic Impedance Spectroscopy (GEIS) of the different GDEs (v1b/CoPc, cyan; v30, greenish brown; v1b/Ag, burgundy), measured at 20 mA cm^{-2}, in the MEA.

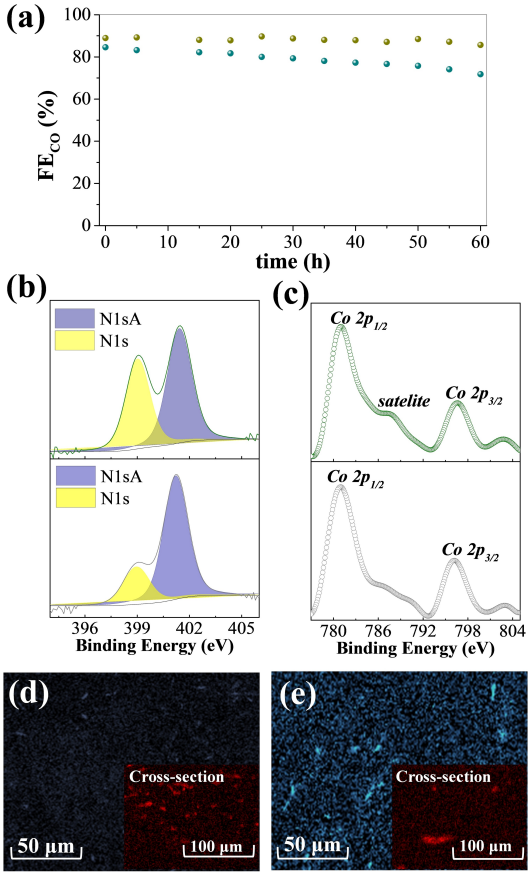

Figure 5. Assessment of ECR stability and post-mortem characterization of the CoPc-functionalized v30 and the CoPc-coated v1 (v1/CoPc) PTLs, in the MEA. (a) Stability of the CoPc functionalized v30 (greenish brown) and the v1/CoPc (cyan) GDEs at a total current density of 100 mA cm^{-2}, (b) N-XPS of the v30 sample after 25 h (grey) and 55 h (green) of continuous ECR, (c) Co-XPS of the v30 sample after 25 h (grey) and 55 h (green) of continuous ECR, (d,e) Co-EDX of the v30 layer and cross-section after 25 h and 55 h of continuous ECR respectively.

potential induced to the MEA cell from the v1/CoPc in comparison with the v1/Ag. The samples present a similar R_{ct} (~4 Ω). The effect is related to the thicker CoPc catalyst layer of the v1/CoPc and the H^+ deprived MEA environment that underlines the CoPc activity (v1/CoPc vs. v30). The v30 presents again the lowest HFR (0.8 Ω) in the MEA cell, derived from the v30 architecture. The v30 low HFR is associated with its low through-plane electrical resistivity (Table S3).

Stability assessment

The high FE_{CO} (90%) selectivity of the v1/CoPc and the v30 GDEs compelled us to investigate their stability in the MEA cell. Applying 100 mA cm^{-2} we recorded a stability of 21 h for the v1/CoPc. Under the same conditions, the v30 GDE recorded a much higher stability, more than 50 h (Figure 5a). We would interpret the increase in the GDE stability as being related to the CoPc-substrate interactions (Figure 2f) and CoPc distribution (Figures 2b,c). Post-mortem XPS analysis (Figure 5b) indicates the attenuation of the CoPc-substrate interactions (N 1s, B), revealing alterations in the coordination state of the CoPc environment. The pyridinic-N interactions (N 1s) of the catalyst tend to increase over the electrolysis runtime. This suggests a tendency for CoPc aggregation. The Co–N interactions (N 1s, A) remain constant indicating a similar environment around the Co-active center of the CoPc. The Co-XPS (Figure 5c) confirms a stable Co-state over the ECR time. The observed satellite in the spectra is related to changes in the e^- density around the Co-center during ECR. SEM and EDX imaging of the surface and the cross-section (Figure 5d,e) of the v30, indicate changes in the original CoPc distribution. Through the time of ECR, CoPc concentration was observed to be depleted from the core of the functionalized v30, gradually migrating towards the surface (Figure S5b). This behavior induces CoPc aggregations over the PTL's surface, a feature intensively observed over the v1/CoPc (Figure S5c). The architecture of the v30 GDE is responsible for delaying the CoPc aggregation (Figure S6a), preventing this deterioration pathway. This feature is responsible for the longer stability of the v30 GDE in the MEA (Figure 5a).

Conclusions

This study presents a significant advancement in the development of non-woven and cost-effective paper-based porous transport layers (PTLs) for CO_2-to-CO conversion. By using both silver and CoPc catalysts, we showcased the adaptability of our substrates with various catalyst materials. We recorded promising ECR performance with our CoPc-coated substrates in a flow-

cell and a membrane electrode assembly (MEA) configuration, reaching a maximum j_{CO} of 180 mA cm^{-2} at low overpotential. The limited stability observed in CoPc gas diffusion electrodes (GDEs) due to catalyst aggregation necessitated further research to enhance cathode efficiency and stability. Using the PGM-free CoPc, we incorporated the catalyst in the initial fabrication process of the substrate. Forming the CoPc-functionalized PTL, designated as "v30," which led to a uniform distribution of the active CoPc catalyst within the substrate. The ECR-active v30, achieved a maximum j_{CO} of 160 mA cm^{-2} at a cell voltage below 3 V, underlining the efficiency of our fabrication approach. The v30 architecture induced CoPc-catalyst interactions, resulting in recording stable ECR at 100 mA cm^{-2} for over 50 hours. Our findings provide a stepping-stone in the fabrication of facile catalytically active GDEs, holding great promise for practical CO_2 reduction applications. By combining a hands-on perspective on sustainable ECR practices and addressing limitations associated with the CoPc phase, this work contributes significantly to the advancement of electrochemical catalysis in the context of CO_2 conversion and its applications.

Experimental Section

Iridium (0)/Iridium (III) oxide nano-powder (IrO_x, nanopowder 99.99%), silver nanopowder (Ag, 99.99%, 20–40 nm) were purchased from Alfa-Aesar and used without any purification. Ultrapure (MiliQ) water was used. Carbon Paper (Freudenberg H23 C6), titanium fibers porous transport layer (Ti-PTL, 500 μm thickness), Nafion (5% wt/wt, alcohol-based), Ni-foam (500 μm thickness) and Carbon Black (Cabot Vulcan XC-72) were purchased from Fuel-Cell Store. Sustainion membrane (X37-50 grade RT) was purchased from Dioxide Materials. Potassium hydroxide (KOH, 99%), cobalt phthalocyanine (CoPc, 99.99%), were purchased from Sigma-Aldrich and used without further purification.

Paper-based PTL fabrication and characterization

To create a CoPc-loaded wet-laid paper of a diameter of 5 cm^2, PTL Set Up v30 was made by lab scale procedure similar to a Rapid Koethen sheet formation according to DIN EN ISO 5269–2, fiber suspension included kraft and eucalyptus pulp and graphite mixture with a contribution of about 80% of the overall paper composition. Additional additives were alkyl ketene dimer (AKD) and a wet strength agent (WSA) in optimized amounts, to enhance the hydrophobicity and stability behavior of the paper PTL especially for the prevention of flooding phenomena under alkaline conditions (1 M KOH) in the flow-cell set up.

PTL set ups v1 and v1b were generated continuously by the pilot paper machine. These samples had a similar composition likewise v30, without catalyst loading. Catalytic functionalization for the machine materials was realized by subsequent spray coating as also mentioned in the electrode fabrication section, while v1b was PTFE coated on the machine's surface side by blade coating (Control Coater K202, Model 624, & Coatmaster, Model 509 MC, Erichsen GmbH & Co. KG) for increasing hydrophobicity for flow-cell operation.

Tensile strength, breaking elongation as deviations of elastic modulus, tensile energy of absorption and tensile strength index of the Paper PTLs were measured according to DIN EN ISO 1924–2 on universal testing machine Inspekt 20 (vertical). The thickness of the paper was determined according to DIN EN ISO 534 on L&W Micrometer SE 250. Tearing resistance (according to Elmendorf) was evaluated according to DIN EN ISO 1974 on L&W Tearing Tester Code 289. Grammage was determined according to DIN EN ISO 536 on analytical balance Sartorius BA 310 P. Air Permeability was measured according to Gurley by ISO 5636–5 on Messmer Gurley-Densometer 4110 TYP 21-C.

Catalyst-coated electrode fabrication

All catalyst-coated gas diffusion electrodes (GDEs) were prepared by depositing the catalyst layer on the substrate using an automatic spray coating machine (Sono-Tek, ExactaCoat). The Ag-ink was composed of 150 mg of commercial Ag-catalyst powder, 12 ml of isopropanol, 7.5 ml of water (Milli-Q), and 158.3 μl of Nafion solution (5% wt/wt). The CoPc-ink was composed of 32 mg CoPc, 324 mg of Carbon Black, 60 ml Acetone, 880 μl of Nafion solution (5% wt/wt). All the different inks were put under Ultra-Turex (33.000 rpm) for 5 min and then into a sonication bath for 60 min before spray-coating. The Ag-GDEs had a loading of 1 mg cm^{-2}, while the CoPc-GDEs had an optimum loading of 0.65 mg cm^{-2} of catalyst. After preparation, all the different GDEs prepared were dried at 70 °C for 3 h. Such heat treatment aims to evaporate the residual surfactants from the ionomer suspension and the dispersive media.

For the MEA anode, a Ti fiber-mesh was used as the PTL (porous transport layer). The original Ti-PTL was etched in concentrated boiling HCl (1 M), to break-down the initial passivating TiO_x layer. The etched PTL was sprayed with IrO_x nanoparticles (Alfa-Aesar) to form the anode catalyst layer. The ink composition used for the anode was: 40 mg of IrO_x and 10 mg of Nafion Ionomer (in ethanolic 5% w/w solution) dispersed in 5 ml methanol. The loading of IrO_x was 2 mg cm^{-2}.

Electrochemical measurements

Electrochemical experiments were performed in a flow-cell (Electro-Cell) with an active area of 1 cm^2. The reference electrode was Ag/AgCl and the applied potentials were related with an RHE using the equation: $E_{RHE} = E_{Ag/AgCl} + 0.059 \times pH + 0.1976$. The electrolyte used was 1 M KOH with a flow rate of 4.6 ml min^{-1}, while the CO_2 was fluxed at 16 sccm. The electrochemical performance was evaluated from the polarization curve of the material in the potential window of −0.4 V to −1.2 V (vs RHE). In the flow cell, the counter electrode was Ni-foam of 0.5 μm thickness. For each point of the polarization curve, the GDE was potentiostatically run for 25 min.

For the measurements of CO_2 reduction in MEA configuration, a customized cell with an active area of 2 cm^2 (1×2 cm^2) was used. The anode was IrO_x/Ti-PTL while the anolyte was 0.1 M $KHCO_3$. Sustainion AEM (X37-50 RT) membrane with a thickness of ~50 microns was used. The CO_2 (30 sccm) was humidified at room temperature before entering the cell. The PTFE gasket used, had 400 μm thickness and the cell was assembled by applying 2 Nm torque. The cathode materials were our developed paper-based substrates coated with either Ag or CoPc catalyst or the commercially available Freudenberg substrate, as comparison media. The catalyst layer of the anode and the cathode were facing the AEM membrane during the assembly of the cell. The polarization curve was produced by leaving the cell running for 25 min at fixed current. During this time the average necessary voltage to maintain the current was assessed and the products were collected after 20 minutes.

For both flow-cell and MEA electrolyzers, the CO_2 reduction products were analyzed using an in-line gas chromatography

(Agilent 490) coupled with a thermal conductivity detector (TCD). Argon and helium gas (99.999% each) were used as carrier gasses.

In the flow-cell the potentiostatic electrochemical impedance spectroscopy (PEIS) was conducted in the range 10 mHz −10 kHz. The PEIS was measured at the onset potential of each GDE, to assess the charge transfer resistance (Rct) induced by the sample. In the MEA, the galvanostatic electrochemical impedance (GEI) of each sample was measured at 20 mA cm^{-2}.

The Faradaic efficiency for gas products was calculated using the following formula:

$$FE\ (\%) = (z \cdot C \cdot V \cdot F \cdot P)/(I \cdot R \cdot T) \quad (1)$$

$$z = \text{number of e for product formation } (2e\text{- for CO}) \quad (2)$$

$$C = \text{concentration of product in the gas-outlet stream} \quad (3)$$

$$V = \text{flowrate of the gas-outlet stream } (\text{sccm}) \quad (4)$$

$$F = 96485\ \text{C mol}^{-1} \quad (5)$$

$$P = 101325\ \text{Pa} \quad (6)$$

$$R = 8.314\ \text{J mol}^{-1}\ \text{K}^{-1} \quad (7)$$

$$T = 298\ \text{K} \quad (8)$$

$$I = \text{total current passed through the cathode} \quad (9)$$

The FE was calculated based on the gas flow-rate measured at the outlet of the flow-cell for the selected points of the polarization curve. The gas product quantification was done using a Tesko Agilent micro GC, coupled with a TCD detector.

The Energy Efficiency for CO (EE_{CO}) of the MEA set-up was calculated according to the following formula: $EE_{CO} = (1.17 \times FE_{CO})/E_{cell}$ where 1.17 V is the thermodynamically required potential for the electrolysis of CO_2 to CO (cathode) and the OER (anode), E_{cell} = the full cell potential in the MEA set-up and FE_{CO} = the Faradaic Efficiency towards CO for each point of operation.

Characterization

The surface composition of the samples was analyzed using X-ray photoelectron spectroscopy (XPS) (Phi5000 VersaProbeII, ULVAC-Phi Inc., USA). The radiation source was Al K-alpha, monochromatic (1.486 keV) with X-ray setting: 50 W, 15 kV, 200 μm spot. The survey spectra were obtained by applying 187.5 eV pass energy, 0.8 eV step, 100 ms/step and the detailed spectra by applying 23.5 eV pass energy, 0.1 eV step, 100 ms/step. The quantification of the surface composition was done by integrating the survey XPS of each sample. For each PTL two different samples underwent survey XPS measurements at two different points of their surface. The standard deviation (SD%) of the elemental composition was calculated according to the value of the integrated peak.

The surface morphology and the elemental distribution were observed through SEM/EDX, using the Zeiss Gemini 500 with EDX (Oxford).

The morphology of the GDEs was observed with a scanning electron microscope (SEM). For this purpose, the Zeiss 1550 VP Scanning Electron Microscope was used with a Gemini column, up to 30 keV.

The inherent hydrophobicity of the fabricated paper-based substrates was assessed with a Kruss DSA25 Drop Shape Analyzer. For the measurement 10 μl of MilliQ water was dropped on the catalyst layer. The measurement of the contact angle was done under static conditions (Cassie-Baxter).

The nitrogen (N_2) specific surface area (SSA) values were calculated according to the Brunauer-Emmett-Teller (BET) method, and were obtained using the Autosorb iQ instrument coupled with ASiQWin 4.0 software. Before the analysis, the samples were thermally treated (degassed) at 150 °C under vacuum.

Supporting Information

Additional references cited in the Supporting Information (Ref. [41–49].

Acknowledgements

We are thankful for the funding of our work, jointly provided by the German Ministry BMBF and the French National Agency for Research ANR under development No. 03SF0586 C (Electrocatalysis for CO_2 conversion into CO, EL-Cat). M.R. acknowledges the Institut Universitaire de France (IUF) for partial financial support.

We are also thankful to Steffen Schramm and his team of the pilot plant section at PTS, for coordinating the machine manufacturing of our novel materials.

Conflict of Interests

The authors declare no conflict of interest.

Data Availability Statement

The data that support the findings of this study are available from the corresponding author upon reasonable request.

Keywords: cobalt phthalocyanine · electrochemical CO_2 reduction · flow-cell · porous transport layer · zero-gap

[1] T. M. Gür, *Prog. Energy Combust. Sci.* **2022**, *89*, 100965.
[2] D. T. Whipple, P. J. A. Kenis, *J. Phys. Chem. Lett.* **2010**, *1*, 3451–3458.
[3] L. Peters, A. Hussain, M. Follmann, T. Melin, M.-B. Hägg, *Chem. Eng. J.* **2011**, *172*, 952–960.
[4] E. V. Kondratenko, G. Mul, J. Baltrusaitis, G. O. Larrazábal, J. Pérez-Ramírez, *Energy Environ. Sci.* **2013**, *6*, 3112–3135.
[5] O. S. Bushuyev, P. De Luna, C. T. Dinh, L. Tao, G. Saur, J. van de Lagemaat, S. O. Kelley, E. H. Sargent, *Joule* **2018**, *2*, 825–832.
[6] S. Dongare, N. Singh, H. Bhunia, P. K. Bajpai, A. K. Das, *ChemistrySelect* **2021**, *6*, 11603–11629.
[7] S. Nitopi, E. Bertheussen, S. B. Scott, X. Liu, A. K. Engstfeld, S. Horch, B. Seger, I. E. L. Stephens, K. Chan, C. Hahn, J. K. Nørskov, T. F. Jaramillo, I. Chorkendorff, *Chem. Rev.* **2019**, *119*, 7610–7672.
[8] Y. Zheng, A. Vasileff, X. Zhou, Y. Jiao, M. Jaroniec, S.-Z. Qiao, *J. Am. Chem. Soc.* **2019**, *141*, 7646–7659.
[9] M. Jouny, W. Luc, F. Jiao, *Ind. Eng. Chem. Res.* **2018**, *57*, 2165–2177.

[10] G. O. Larrazábal, A. J. Martín, J. Pérez-Ramírez, *J. Phys. Chem. Lett.* **2017**, *8*, 3933–3944.
[11] S. Verma, B. Kim, H.-R. "Molly" Jhong, S. Ma, P. J. A. Kenis, *ChemSusChem* **2016**, *9*, 1972–1979.
[12] J. M. Spurgeon, B. Kumar, *Energy Environ. Sci.* **2018**, *11*, 1536–1551.
[13] E. W. Lees, B. A. W. Mowbray, F. G. L. Parlane, C. P. Berlinguette, *Nat. Rev. Mater.* **2022**, *7*, 55–64.
[14] C.-T. Dinh, F. P. García de Arquer, D. Sinton, E. H. Sargent, *ACS Energy Lett.* **2018**, *3*, 2835–2840.
[15] Y. Chen, C. W. Li, M. W. Kanan, *J. Am. Chem. Soc.* **2012**, *134*, 19969–19972.
[16] I. Stamatelos, C.-T. Dinh, W. Lehnert, M. Shviro, *ACS Appl. Energ. Mater.* **2022**, *5*, 13928–13938.
[17] S. Sarfraz, A. T. Garcia-Esparza, A. Jedidi, L. Cavallo, K. Takanabe, *ACS Catal.* **2016**, *6*, 2842–2851.
[18] M. Asadi, B. Kumar, A. Behranginia, B. A. Rosen, A. Baskin, N. Repnin, D. Pisasale, P. Phillips, W. Zhu, R. Haasch, R. F. Klie, P. Král, J. Abiade, A. Salehi-Khojin, *Nat. Commun.* **2014**, *5*, 4470.
[19] K. Takahashi, K. Hiratsuka, H. Sasaki, S. Toshima, *Chem. Lett.* **1979**, *8*, 305–308.
[20] S. Meshitsuka, M. Ichikawa, K. Tamaru, *J. Chem. Soc., Chem. Commun.* **1974**, *5*, 158–159.
[21] C. Costentin, S. Drouet, M. Robert, J.-M. Savéant, *Science* **2012**, *338*, 90–94.
[22] Z. Weng, J. Jiang, Y. Wu, Z. Wu, X. Guo, K. L. Materna, W. Liu, V. S. Batista, G. W. Brudvig, H. Wang, *J. Am. Chem. Soc.* **2016**, *138*, 8076–8079.
[23] X. Zhang, Z. Wu, X. Zhang, L. Li, Y. Li, H. Xu, X. Li, X. Yu, Z. Zhang, Y. Liang, H. Wang, *Nat. Commun.* **2017**, *8*, 14675.
[24] M. Wang, K. Torbensen, D. Salvatore, S. Ren, D. Joulié, F. Dumoulin, D. Mendoza, B. Lassalle-Kaiser, U. Işci, C. P. Berlinguette, M. Robert, *Nat. Commun.* **2019**, *10*, 3602.
[25] S. Ren, D. Joulié, D. Salvatore, K. Torbensen, M. Wang, M. Robert, C. P. Berlinguette, *Science* **2019**, *365*, 367–369.
[26] N. Li, W. Lu, K. Pei, W. Chen, *RSC Adv.* **2015**, *5*, 9374–9380.
[27] J. J. Kaczur, H. Yang, Z. Liu, S. D. Sajjad, R. I. Masel, *Front. Chem.* **2018**, *6 (263)*, 2296–2646.
[28] J. Herranz, A. Pătru, E. Fabbri, T. J. Schmidt, *Curr. Opin. Electrochem.* **2020**, *23*, 89–95.
[29] S. Ghoshal, S. Zaccarine, G. C. Anderson, M. B. Martinez, K. E. Hurst, S. Pylypenko, B. S. Pivovar, S. M. Alia, *ACS Appl. Energ. Mater.* **2019**, *2*, 5568–5576.
[30] R. I. Masel, Z. Liu, H. Yang, J. J. Kaczur, D. Carrillo, S. Ren, D. Salvatore, C. P. Berlinguette, *Nat. Nanotechnol.* **2021**, *16*, 118–128.
[31] D. P. Leonard, R. L. Borup, *Meet. Abstr.* **2019**, *MA2019-02*, 1426.
[32] M. F. Mathias, J. Roth, J. Fleming, W. Lehnert, Diffusion Media Material and Characterization, Handbook of Fuel Cells-Fundamentals, Technology and Applications, John Wiley & Sons, Ltd, **2010**, *3*, 517–537.
[33] L. Isikel, I. Gocek, S. Adanur, *The Journal of The Textile Institute* **2010**, *101*, 1006–1014.
[34] B. Yarar Kaplan, L. Işıkel Şanlı, S. Alkan Gürsel, *J. Mater. Sci.* **2017**, *52*, 4968–4976.
[35] A. J. Navarro, M. A. Gómez, L. Daza, J. J. López-Cascales, *Sci. Rep.* **2022**, *12*, 4219.
[36] A. A. Samu, I. Szenti, Á. Kukovecz, B. Endrődi, C. Janáky, *Commun. Chem.* **2023**, *6*, 1–9.
[37] J. Rosen, G. S. Hutchings, Q. Lu, S. Rivera, Y. Zhou, D. G. Vlachos, F. Jiao, *ACS Catal.* **2015**, *5*, 4293–4299.
[38] J. Macko, N. Podrojková, R. Oriňaková, A. Oriňak, *Nanomater. Nanotechnol.* **2022**, *12*, 18479804211062316.
[39] X. Kong, G. Liu, S. Tian, S. Bu, Q. Gao, B. Liu, C.-S. Lee, P. Wang, W. Zhang, *Small* **2022**, *18*, 2204615.
[40] J. Bonin, A. Maurin, M. Robert, *Coord. Chem. Rev.* **2017**, *334*, 184–198.
[41] J. Choi, P. Wagner, R. Jalili, J. Kim, D. R. MacFarlane, G. G. Wallace, D. L. Officer, *Adv. Energy Mater.* **2018**, *8*, 1801280.
[42] H. Li, Y. Pan, Z. Wang, Y. Yu, J. Xiong, H. Du, J. Lai, L. Wang, S. Feng, *Nano Res.* **2022**, *15*, 3056–3064.
[43] N. Han, Y. Wang, L. Ma, J. Wen, J. Li, H. Zheng, K. Nie, X. Wang, F. Zhao, Y. Li, J. Fan, J. Zhong, T. Wu, D. J. Miller, J. Lu, S.-T. Lee, Y. Li, *Chem* **2017**, *3*, 652–664.
[44] M. Huai, Z. Yin, F. Wei, G. Wang, L. Xiao, J. Lu, L. Zhuang, *Chem. Phys. Lett.* **2020**, *754*, 137655.
[45] K. Torbensen, C. Han, B. Boudy, N. von Wolff, C. Bertail, W. Braun, M. Robert, *Chem. Eur. J.* **2020**, *26*, 3034–3038.
[46] M. Abdinejad, C. Dao, X. Zhang, H. B. Kraatz, *J. Energy Chem.* **2021**, *58*, 162–169.
[47] D. A. Salvatore, D. M. Weekes, J. He, K. E. Dettelbach, Y. C. Li, T. E. Mallouk, C. P. Berlinguette, *ACS Energy Lett.* **2018**, *3*, 149–154.
[48] X. Zhang, Y. Wang, M. Gu, M. Wang, Z. Zhang, W. Pan, Z. Jiang, H. Zheng, M. Lucero, H. Wang, G. E. Sterbinsky, Q. Ma, Y.-G. Wang, Z. Feng, J. Li, H. Dai, Y. Liang, *Nat. Energy* **2020**, *5*, 684–692.
[49] H.-Y. Jeong, M. Balamurugan, V. S. K. Choutipalli, E. Jeong, V. Subramanian, U. Sim, K. T. Nam, *J. Mater. Chem. A* **2019**, *7*, 10651–10661.

Manuscript received: August 1, 2023
Revised manuscript received: October 12, 2023
Accepted manuscript online: November 17, 2023
Version of record online: December 14, 2023